ACS OMEGA

http://pubs.acs.org/journal/acsodf

Article

# Flexible Graphene-Assembled Film-Based Antenna for Wireless Wearable Sensor with Miniaturized Size and High Sensitivity

Jibo Zhang,[§] Rongguo Song,[§] Xin Zhao, Ran Fang, Bin Zhang, Wei Qian, Jingwei Zhang, Chengguo Liu,* and Daping He*

Cite This: *ACS Omega* 2020, 5, 12937−12943

Read Online

ACCESS | Metrics & More | Article Recommendations | Supporting Information

**ABSTRACT:** The flexible radio frequency (RF) wireless antennas used as sensors, which can detect signal variation resulting from the deformation of the antenna, have attracted increasing attention with the development of wearable electronic devices and the Internet of Things (IoT). However, miniaturization and sensitivity issues restrict the development of flexible RF sensors. In this work, we demonstrate the application of a flexible and highly conductive graphene-assembled film (GAF) for antenna design. The GAF with a high conductivity of $10^6$ S/m has the advantages of light weight, high flexibility, and superb mechanical stability. As a result, a small-size (50 mm × 50 mm) and flexible GAF-based antenna operating at 3.13−4.42 GHz is achieved, and this GAF antenna-based wireless wearable sensor shows high strain sensitivities of 34.9 for tensile bending and 35.6 for compressive bending. Furthermore, this sensor exhibits good mechanical flexibility and structural stability after a 100-cycle bending test when attached to the back of the hand and the wrist, which demonstrates broad application prospects in health-monitoring devices, electronic skins, and smart robotics.

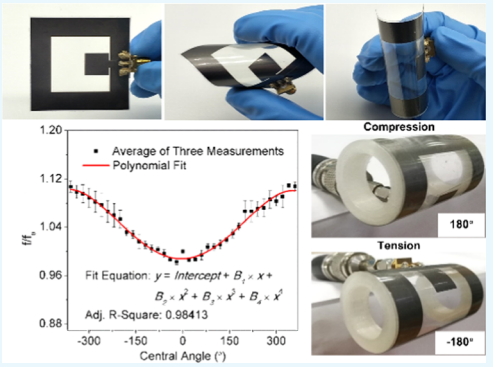


## INTRODUCTION

With the rapid development of Internet of Things (IoT) and the increasing popularity of wearable electronic devices, flexible sensors have received considerable attention. They have been widely used in electronic skin equipment,[1] human motion detection,[2] human health monitoring,[3] and implantable medical devices.[4] Flexible sensors are mainly classified into piezoresistive sensors,[5] capacitive sensors,[6] and piezoelectric sensors[7] according to their working principles. In addition to the above-mentioned three traditional working principles, flexible radio frequency (RF) sensors, which can detect signal variation resulting from the deformation of the antenna, have attracted increasing attention due to the new working principle.[8] In recent years, the development of flexible RF sensors, according to the different antenna structures, can be generally divided into microstrip patch antenna sensors and radio frequency identification (RFID) tag sensors, such as a microstrip patch antenna sensor operating at 5.8 GHz,[9] a rectangular patch antenna sensor operating at 3 GHz,[10] and a ultrahigh-frequency RFID tag sensor.[11] However, relying solely on the optimization of the antenna structure, the improvement of the sensitivity of the flexible RF sensor is still limited. Developing a material with excellent properties for manufacturing sensors is also extremely crucial.

Metals are commonly used in the existing commercial RF sensors.[12−15] However, these materials suffer from poor flexibility, high density, and easy corrosion, which hinder their further applications in flexible RF sensors and make it urgent to find new alternative materials. Recently, conductive polymers[16,17] and carbon materials[18−20] including carbon nanoparticles,[21] carbon nanowires,[22] carbon nanotubes,[23] and graphite[24] have been receiving more attention. Compared to metals, these materials are endowed with properties like light weight and great flexibility but with the sacrifice of conductivity. Graphene, a new generation of carbon material, is shown to be a good candidate for flexible RF sensors.[25−30] In addition to the common features of conductive polymers and carbon materials, it also offers a distinct advantage in terms of electrical conductivity. Graphene-assembled film (GAF) with multilayer sheets, compared to mono- or few-layer graphene films, is attracting more attention due to its high electrical conductivity and low sheet resistance.[31−37] In 2018, we first reported that the GAF-based flexible RF sensor has a higher stability and sensitivity than the copper foil-based antenna sensor with the same size due to the material properties.[38] However, the sensitivity and miniaturization of GAF-based

Received: February 17, 2020
Accepted: May 11, 2020
Published: May 30, 2020

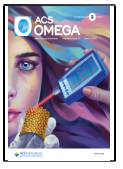









https://dx.doi.org/10.1021/acsomega.0c00263
*ACS Omega* 2020, 5, 12937−12943

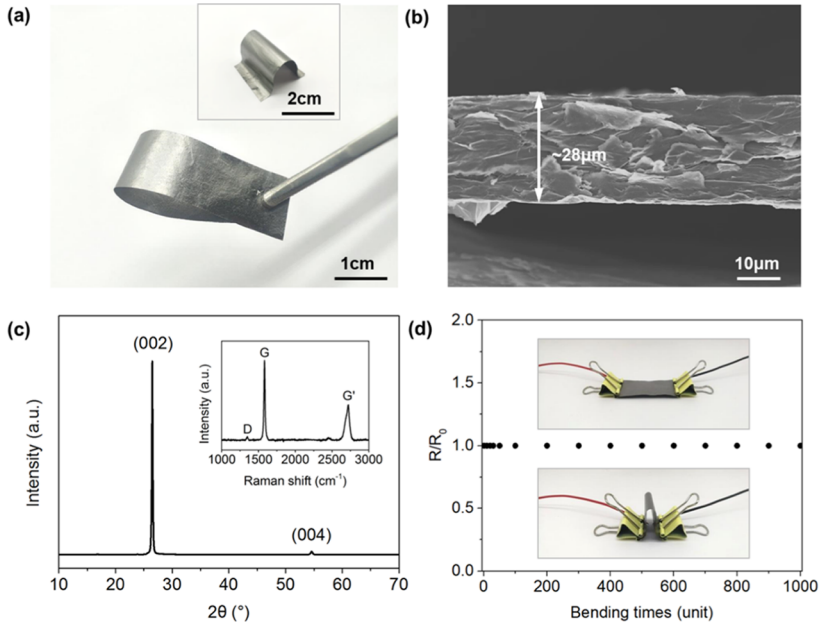


**Figure 1.** Characterization of GAF. (a) Digital photo of GAF with good flexibility. (b) Cross-sectional scanning electron microscopy (SEM) image of GAF with a thickness of 28 $\mu$m (scale bar: 10 $\mu$m). (c) X-ray diffraction pattern and Raman spectrum (inset) of GAF. (d) Mechanical stability test of GAF.

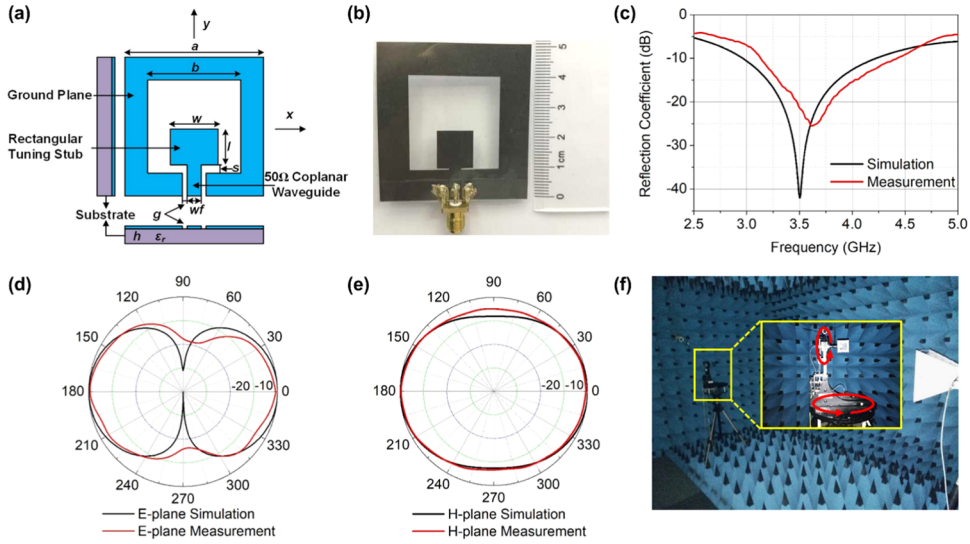


**Figure 2.** Structure and performance measurement of GAF antenna. (a) Schematic of GAF antenna. (b) Photograph of GAF antenna. (c) Simulated (black) and measured (red) reflection coefficient of GAF antenna. (d, e) Comparison of the simulated and measured results of GAF antenna in the E-plane and H-plane, respectively. (f) Measurement environment of the radiation patterns of GAF antenna (Inset: zoomed-in image of the positioner platform with the red arrow showing the rotating direction).

flexible RF sensor need to be further improved to meet the requirements of wearable electronic devices.

In this work, we present a flexible RF sensor based on GAF coplanar waveguide (CPW) antenna with a very small size (dimension of 50 mm × 50 mm). High-conductivity GAF, fabricated by high-temperature heat treatment and rolling compression process, achieves a conductivity of up to $10^6$ S/m and a thickness of 28 $\mu$m and is used to create a flexible antenna for wireless wearable sensors. The miniaturized antenna structure is designed according to the theory of transmission lines with the antenna model built and optimized by electromagnetic simulation software. The return loss of GAF antenna fabricated by the laser direct molding engraving machine is measured by a network analyzer with the radiation patterns obtained by an antenna measurement system. To improve the measurement precision of strain sensing of the flexible RF sensor, we use poly(lactic acid) (PLA) rings of different radii as testing fixtures, and the radii of the rings are set so that the central angle changes precisely with a step size of 10°. The flexible RF sensor shows a tunable resonant frequency dependent on the applied strains as well as outstanding stability and durability under 100 cycles of bending test when attached to the human body. Comparing the proposed sensor with bending strain antenna sensors reported in the literature, the former shows a higher sensitivity with a smaller size. In addition, this flexible GAF antenna


https://dx.doi.org/10.1021/acsomega.0c00263
ACS Omega 2020, 5, 12937−12943

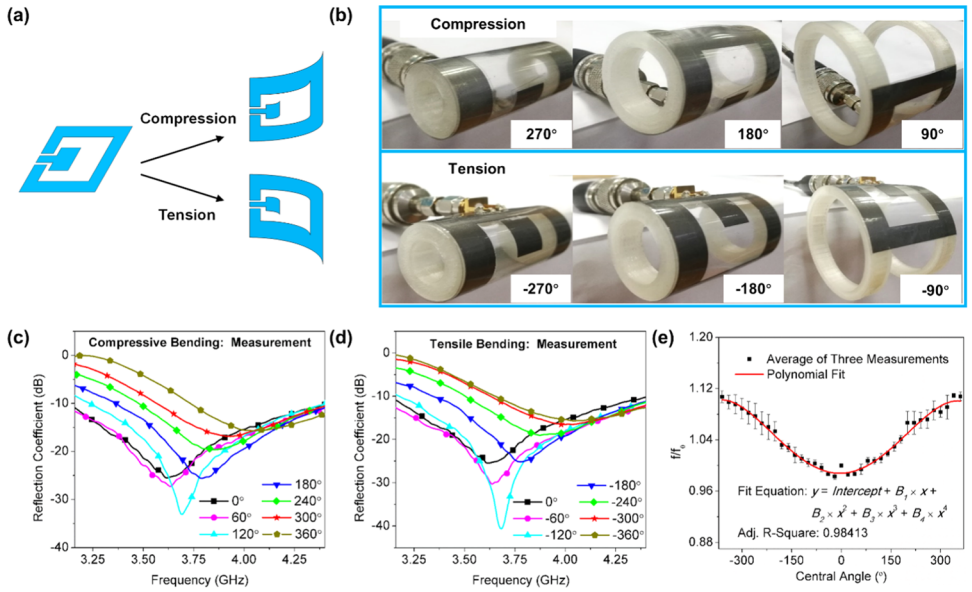


**Figure 3.** Strain measurement of flexible antenna sensor. (a) Schematic of sensor bending under compression and tension. (b) Representative images of GAF sensor conformed to poly(lactic acid) (PLA) rings with different radii. (c, d) Reflection coefficient of antenna as a function of frequency under compressive bending (c) and tensile bending (d) for different central angles. (e) Normalized resonant frequency of flexible antenna sensor as a function of the central angle. The measured results of the antenna with these two statuses (compressive bending and tensile bending) display a similar trend.

operating at 3.13−4.42 GHz is available to the 5G mobile communication.

## RESULTS AND DISCUSSION

The GAF prepared using the method described above shows excellent flexibility, as shown in Figure 1a. The scanning electron microscopy (SEM) image of the cross section (Figure 1b) exhibits a uniform thickness of ∼28 $\mu$m. The X-ray diffraction (XRD) pattern shown in Figure 1c exhibits a sharp and intense characteristic peak located at $2\theta$ = 26.5°, which indicates that the GAF with $d_{002}$ = 0.34 nm has a regular graphene-layered stack structure. In addition, the diffraction peak (004) proves the high graphitization structure of GAF. The little D band (1335 $cm^{-1}$) and the sharp G band (1585 $cm^{-1}$) in the Raman spectra in the inset of Figure 1c indicate that the GAF has few lattice defects and a highly $sp^2$-hybridized carbon atom structure. To verify the mechanical stability, the resistance of GAF is tested after bending. As shown in Figure 1d, the resistance remains unchanged after 1000 times bending, indicating that the GAF has excellent stability under large-scale mechanical deformation.

To ensure the flexibility of the antenna sensor, poly(ethylene terephthalate) (PET) is chosen as the substrate due to its high elasticity and decent dielectric properties. Figure 2a shows the side-view, top-view, and front-view schematics of the GAF antenna. The antenna consists of two layers. The upper layer is a 0.028 mm thick GAF with an electrical conductivity of 1.1 × $10^6$ S/m. The bottom layer is a flexible PET substrate with a thickness $h$ of 0.06 mm and a relative dielectric constant $\varepsilon_r$ of 3.5. The overall size of the antenna $a \times a$ is 50 mm × 50 mm. A square slot with a side length $b$ of 30 mm is formed in the antenna radiator to expand the bandwidth so that the bandwidth of antenna covers a part of the 5G frequency band. A rectangular short tuning stub is used to adjust the resonant frequency and impedance of the antenna. The length $l$ and width $w$ of the tuning stub are 12.047 and 12.045 mm, respectively. The spacing $s$ between the short side of the tuning stub and the square slot is 0.53 mm. A CPW with the advantages of small size, light weight, and low profile[39] is designed to feed the antenna. With the special feed structure, the problem of narrow matching line is solved, thus making it very suitable for the feeding of the thin-substrate antenna. In addition, the CPW structure has a significant advantage in miniaturization of the antenna sensors because the center strip and ground strip are integrated into one plane. A ratio of the center conductor strip width $wf$ of 4 mm and a gap width $g$ of 0.13 mm between the center conductor strip and the ground plane are chosen to ensure that the input impedance of the feeder port is 50 Ω (the simulation results of reflection coefficients of the antenna with different parameters are shown in Figure S1, and the simulation results of the surface current of the antenna are shown in Figure S2, Supporting Information).

Figure 2b shows the digital photo of a GAF antenna. The simulated and measured reflection coefficients of the antenna shown in Figure 2c are in good agreement. The measured reflection coefficient of the antenna at the resonant frequency of 3.62 GHz is −25.47 dB, and the −10 dB bandwidth is 3.13−4.42 GHz, which are applicable to the sub-6 GHz band of 5G. Due to the insufficient machining accuracy and manual welding of Sub-Miniature-A (SMA), the input impedance of the actual antenna is slightly different from that of the design. The relationship between the reflection coefficient $S_{11}$ and the input impedance $Z_{in}$ of the antenna is shown in eq 1.

$$|S_{11}|\,(\mathrm{dB}) = 20 \log \left| \frac{Z_{in} - Z_0}{Z_{in} + Z_0} \right| \quad (1)$$

where $Z_0$ represents the characteristic impedance 50 Ω of the transmission line. The discrepancy between the measured and simulated reflection coefficients is essentially derived from the difference in input impedance. Figure 2d,e shows the simulated and measured radiation patterns of the GAF antenna in the E-


https://dx.doi.org/10.1021/acsomega.0c00263
ACS Omega 2020, 5, 12937−12943

Table 1. Comparison of the Proposed Sensor with Bending Strain Antenna Sensors Reported in the Literature

| material | radiator conductivity (S/m) | maximum sensitivity | size (mm) | reference |
|---|---|---|---|---|
| aluminum/paper | $3.56 \times 10^7$ | 3.34 | a cylinder with a diameter of ∼65.5 mm and a height of 0.2 mm | 40 |
| copper/cellulose paper | $1.30 \times 10^7$ | 5.39 | 119.4 × 70 × 0.46 | 38 |
| graphene/cellulose paper | $\sim 10^6$ | 9.8 | 119.4 × 70 × 0.46 | 38 |
| graphene/poly(ethylene terephthalate) | $\sim 10^6$ | 35.6 | 50 × 50 × 0.088 | this work |

plane and H-plane at their resonant frequencies. The measured radiation patterns of the antenna are similar to the simulated results. It can be clearly seen from Figure 2d,e that the maximum radiation directions of the antenna in the E-plane are 0 and 180°, and the radiation in the H-plane is omnidirectional. The external SMA connector whose length is about one-third of the antenna during the antenna test affects the radiation of the antenna, resulting in the discrepancy between the measured and simulated radiation patterns. The far-field characteristics are tested in a microwave anechoic chamber with a network analyzer (PNA, Keysight N5247A), as shown in Figure 2f, while the E-plane and H-plane of the antenna are measured by rotating the positioner platform 360° horizontally and vertically, respectively.

The flexible GAF antenna can be viewed as a strain sensor, as shown in Figure 3a. The sensor is bent toward the radiation patch when it is under compression, and it is bent toward the substrate when it is under tension. To measure the mechanical flexibility of the GAF antenna sensor, it is conformed to PLA rings with different radii, as shown in Figure 3b. There is a one-to-one corresponding relationship between the central angle of the antenna conformed to the rings and the radius of the rings, and the radii of the rings are set so that the central angle changes with a step size of 10°. Figure 3c,d shows the reflection coefficient of antenna as a function of frequency under compressive bending and tensile bending for different central angles. For both compressive bending and tensile bending, the resonant frequency of the antenna gradually increases as the bending angle increases. The result can be explained by eqs 2 and 3.

$$r = \frac{a}{\theta} \tag{2}$$

$$f = \frac{c}{2(l + 2\Delta l)\sqrt{\varepsilon_e}} \tag{3}$$

where $c$ is the speed of light in free space, $f$ is the resonant frequency of antenna, $\varepsilon_e$ is the effective dielectric constant derived from the dielectric constants of PET substrate and air, and $\Delta l$ is the extended length of the patch because the presence of the edge effect makes the actual effective length larger than the physical length of the patch.

Equation 2 indicates an inverse relationship between the bending radius $r$ and the central angle $\theta$. Equation 3 is a transformation of eq 6 of antenna design equations and shows that the resonant frequency $f$ and effective length of the radiation patch $l + 2\Delta l$ are inversely proportional.

Figure S3 in the Supporting Information shows the geometric structures of the antenna before and after bending. The antenna in the unbent state can be approximated as a plane; $a$ is the length of the bent side of the antenna, and $l + 2\Delta l$ is the effective length of the patch. When the antenna is being bent, it can be equivalent to another plane; $a'$ is the equivalent length of the bent side of the antenna, and $l' + 2\Delta l'$ is the equivalent effective length of the patch. It can be clearly seen from Figure S3 that the effective length of the patch becomes smaller after the antenna is bent. According to eq 2, as the absolute value of the central angle $\theta$ gradually increases, the bending radius $r$ decreases accordingly. When $r$ decreases, the effective length of the patch $l + 2\Delta l$ decreases. The resonant frequency increases according to eq 3. Therefore, the resonant frequency $f$ increases as the absolute value of the central angle $\theta$ increases, which is also consistent with the experimental observations shown in Figure 3e.

Three antennas are manufactured, and their resonant frequencies are 3.62, 3.62, and 3.64 GHz through testing. Since the resonant frequency of the first antenna is repeatable and closer to the design frequency of 3.5 GHz, the first antenna is used for bending measurement. We perform three repeated bending measurements on the antenna that show similar results. Figure 3e shows the average of the three measurements. It proves the stability of the GAF sensor and the repeatability of experimental results. According to the distribution of discrete data points, the second-, third-, fourth-, and fifth-order polynomial fittings are performed on the points. Among these fitting curves, the $R^2$ value of the fourth-order fitting is the highest and the fitting curve is within the standard deviation, which is the most suitable for the discrete points distribution. Therefore, the curve in Figure 3e is obtained by fitting the data with quartic polynomial, and the fitting equation is $y = \text{Intercept} + B_1 \times x + B_2 \times x^2 + B_3 \times x^3 + B_4 \times x^4$, where Intercept = 0.98792, $B_1 = 1.57201 \times 10^{-5}$, $B_2 = 1.7897 \times 10^{-6}$, $B_3 = -1.41667 \times 10^{-10}$, $B_4 = -7.04424 \times 10^{-12}$. The goodness of fit can be proved by Adj. $R^2$ of 0.98413. Figure 3e shows the normalized resonant frequency as a function of the central angle when the antenna sensor is bent toward the radiation patch ($\theta > 0°$) and toward the substrate ($\theta < 0°$). When the absolute value of central angle $\theta$ increases, the normalized resonant frequency $f/f_0$ increases, where $f$ is the resonant frequency in the bending state and $f_0$ is the resonant frequency in the relaxed state. The sensitivity $S$ of the antenna sensor can be calculated by the following formulas[40]

$$S = (\Delta f/f_0)/\Delta\xi \tag{4}$$

$$\xi = (\pm)h/2r \tag{5}$$

where $\Delta f$ is the variation of resonant frequency with $\Delta f = f - f_0$, $\xi$ is the bending strain of the sensor, $h$ is the thickness of the PET substrate, and $r$ is the bending radius. The sensitivity $S$ of the antenna sensor is about 34.9 for tensile bending and 35.6 for compressive bending. Comparing the proposed sensor with bending strain antenna sensors reported in the literature, the former exhibits a higher sensitivity with a smaller size, as shown in Table 1.

It is shown that the sensitivities of the antenna sensor for tensile bending and compressive bending are almost identical,


https://dx.doi.org/10.1021/acsomega.0c00263
ACS Omega 2020, 5, 12937−12943

which is determined by the radiation characteristics of the CPW antenna, as shown in Figure 2d,e. For the general antenna with metal ground plate, the ground plate reflects the electromagnetic wave so that the back lobe of the radiation pattern of the antenna is suppressed, and the directivity is improved. However, the center conductor strip and the ground plate of the CPW structure are in one plane. The radiation patterns of the antenna are identical in both upper and lower portions. Therefore, regardless of the tensile bending or compressive bending, the resonant frequency of the antenna shifts uniformly and the sensitivity test results of the antenna with these two statuses display a similar trend.

In Figure 3e, the resonant frequency of the antenna is reduced with the absolute value of central angle increasing from 0 to 60°. One possible reason for this is that the size of the test ring is very large when the angle is small. This causes the antenna to be overstressed, which affects the radiation characteristics of the antenna. In addition, Figure S4a,b shows the reflection coefficient of the antenna as a function of increasing central angle with a step size of 30°.

In addition to the sensitivity test, a flexible antenna sensor is attached to the back of the hand and wrist of a human subject for stability test. Figure 4a,b shows the antenna sensor attached to the back of the hand. The antenna sensor is changed from its initial flat state to a bending state when the subject is making a fist. In Figure 4c,d, the antenna sensor is attached to the subject's wrist. As the wrist bends, the antenna sensor is changed from an initial flat state to a bending state. The antenna sensor is subjected to a 100-cycle test for bending, with the results shown in Figure 4e. It can be clearly seen that the resonant frequency of the antenna changes abruptly with bending but always restores to its original frequency after each bending cycle. This proves the high stability of the flexible antenna sensor and makes it promising for applications[41,42] in the fields of human motion detection, human health monitoring, realizing real-time monitoring of human motion, and physiological activities (photographs of a GAF antenna sensor in different statuses shown in Figure S5, Supporting Information).

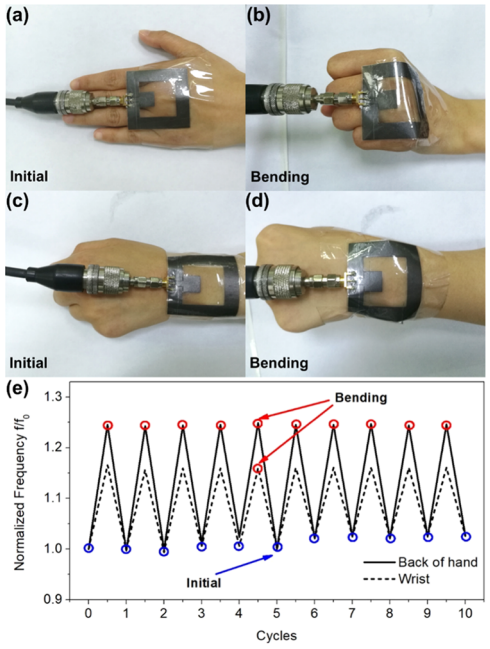


**Figure 4.** Application of flexible antenna sensor for human motion detection. (a, b) Photographs of a flexible antenna sensor attached to the back of the hand in the initial (a) and bending (b) states. (c, d) Photographs of flexible antenna sensor attached to the wrist in the initial (c) and bending (d) states. (e) Response of normalized frequency varying with initial and bending states in the two cases. The normalized frequency changes abruptly but always restores to its original frequency after each bending cycle.

## CONCLUSIONS

In this manuscript, a high-performance wireless wearable RF sensor based on flexible graphene-assembled film antenna has been investigated. In particular, we demonstrated through simulation that the flexible antenna shows good omnidirectional radiation and operates within the frequency range suitable for 5G communication. We verified the results of simulation through experimental analyses of PNA and microwave anechoic chamber, indicating an operation frequency of 3.13−4.42 GHz, which is in good agreement with the simulation results. The sensing characteristics of the flexible RF sensor under tension and compression were also measured and showed high sensitivities of 34.9 and 35.6 under tensile and compressive bendings, respectively. Moreover, with the size of the sensor of 50 mm × 50 mm fed by coplanar waveguide, the miniaturization of the sensor was realized. We also tested the durability of flexible RF sensor by attaching the sensor to the human object and observed good stability. A rationally designed flexible RF sensor with the above merits could contribute to overcome many key limitations of the current sensors and can have applications in human health detection, human motion detection, electronic skin equipment, and other fields.

## EXPERIMENTAL SECTION

**Preparation of GAF.** An aqueous dispersion of graphene oxide (GO) sheets with a concentration of 16 mg/mL was purchased from Wuxi Chengyi Education Technology Co. Ltd. It was first uniformly coated onto poly(ethylene terephthalate) (PET) substrates and then dried at room temperature to obtain GO films. The GO films peeled from PET substrate were annealed at 1300 °C for 2 h and 2800 °C for 1 h subsequently in an argon atmosphere in a high-temperature graphitization furnace. Finally, the films were roll-compressed under 200 MPa to obtain the GAF.

**Characterization.** Microstructural cross-sectional information was imaged with a JEOL JSM-7610F field emission scanning electron microscope (FESEM). X-ray diffraction (XRD) measurements were performed on a Rigaku Smartlab SE instrument using Ni-filtered Cu K$\alpha$ radiation. Raman spectra were recorded by a LabRAM HR Evolution Raman Spectrometer.

**Device Design and Fabrication.** The resonant frequency of the antenna is designed to be at 3.5 GHz to meet the requirements of 5G mobile communication for antenna. The electromagnetic field characteristics of the antenna are analyzed by the transmission line model method, and the physical parameters of the antenna are designed according to eqs 6−9.[43]

$$l = \frac{c}{2f\sqrt{\varepsilon_e}} - 2\Delta l \tag{6}$$


https://dx.doi.org/10.1021/acsomega.0c00263
ACS Omega 2020, 5, 12937−12943

$$w = \frac{c}{2f}\left(\frac{\varepsilon_r + 1}{2}\right)^{-1/2} \quad (7)$$

$$\varepsilon_e = \frac{\varepsilon_r + 1}{2} + \frac{\varepsilon_r - 1}{2}\left(1 + 12\frac{h}{w}\right)^{-1/2} \quad (8)$$

$$\Delta l = 0.412h\frac{(\varepsilon_e + 0.3)\left(\frac{w}{h} + 0.264\right)}{(\varepsilon_e - 0.258)\left(\frac{w}{h} + 0.8\right)} \quad (9)$$

The GAF antenna sensor was fabricated by engraving a specific shape on a GAF-coated PET film using the laser direct molding engraving machine (LPKF ProtoLaser S) (the fabrication device is shown in Figure S6a, Supporting Information).[44]

**Measurement.** The feeder port of antenna was connected to a Sub-Miniature-A (SMA) connector, which was linked to a network analyzer (PNA) through a coaxial line. The resonant frequency and return loss were measured by the PNA. The radiation patterns of the antenna were derived from the antenna measurement system, which consisted of a PNA, a Diamond Engineering Antenna Measurement System (DAMS) platform controller, and a microwave anechoic chamber. The PNA was connected to a positioner platform and a standard reference antenna (REF antenna) of the microwave anechoic chamber to control signal reception. The DAMS platform controller was connected to the positioner platform of the microwave anechoic chamber (the measurement environment is shown in Figure S6b,c, Supporting Information). The radiation patterns were obtained by a rotating antenna under test (AUT) with increments of 10°. The sensing characteristics of the sensor were measured by PNA, while the sensor was conformed to the poly(lactic acid) (PLA) rings of different radii made by the three-dimensional printing technology (the fabrication scheme of the PLA fixture is shown in Figure S7, Supporting Information).

## ■ ASSOCIATED CONTENT

### Supporting Information

The Supporting Information is available free of charge at https://pubs.acs.org/doi/10.1021/acsomega.0c00263.

Simulation results of reflection coefficients of the antenna with different parameters; simulation results of surface current of the antenna; geometric structures of the antenna before and after bending; reflection coefficient of the antenna as a function of increasing central angle with a step size of 30°; photographs of a GAF antenna sensor in different statuses; fabrication device and measurement environment; and fabrication scheme of the PLA fixture (PDF)

## ■ AUTHOR INFORMATION


### Corresponding Authors

**Chengguo Liu** − *Hubei Engineering Research Center of RF-Microwave Technology and Application, School of Science, Wuhan University of Technology, Wuhan 430070, P. R. China*; Phone: +86 139 86111739; Email: liucg@whut.edu.cn

**Daping He** − *Hubei Engineering Research Center of RF-Microwave Technology and Application, School of Science and State Key Laboratory of Advanced Technology for Materials Synthesis and Processing, Wuhan University of Technology, Wuhan 430070, P. R. China*; orcid.org/0000-0002-0284-4990; Phone: +86 177 64000852; Email: hedaping@whut.edu.cn

### Authors

**Jibo Zhang** − *Hubei Engineering Research Center of RF-Microwave Technology and Application, School of Science, Wuhan University of Technology, Wuhan 430070, P. R. China*

**Rongguo Song** − *Hubei Engineering Research Center of RF-Microwave Technology and Application, School of Science, Wuhan University of Technology, Wuhan 430070, P. R. China*

**Xin Zhao** − *Hubei Engineering Research Center of RF-Microwave Technology and Application, School of Science, Wuhan University of Technology, Wuhan 430070, P. R. China*

**Ran Fang** − *Hubei Engineering Research Center of RF-Microwave Technology and Application, School of Science, Wuhan University of Technology, Wuhan 430070, P. R. China*

**Bin Zhang** − *Hubei Engineering Research Center of RF-Microwave Technology and Application, School of Science, Wuhan University of Technology, Wuhan 430070, P. R. China*

**Wei Qian** − *Hubei Engineering Research Center of RF-Microwave Technology and Application, School of Science, Wuhan University of Technology, Wuhan 430070, P. R. China*

**Jingwei Zhang** − *Hubei Engineering Research Center of RF-Microwave Technology and Application, School of Science, Wuhan University of Technology, Wuhan 430070, P. R. China*

Complete contact information is available at: https://pubs.acs.org/10.1021/acsomega.0c00263

### Author Contributions

§J.Z. and R.S. contributed equally to this work.


### Notes

The authors declare no competing financial interest.

## ■ ACKNOWLEDGMENTS

This work was supported by the National Natural Science Foundation of China (51672204 and 51701146) and Foundation of National Key Laboratory on Electromagnetic Environment Effects (No. 614220504030617).

## ■ REFERENCES


(1) Lou, Z.; Chen, S.; Wang, L.; Jiang, K.; Shen, G. An Ultra-Sensitive and Rapid Response Speed Graphene Pressure Sensors for Electronic Skin and Health Monitoring. *Nano Energy* **2016**, *23*, 7−14.

(2) Yamada, T.; Hayamizu, Y.; Yamamoto, Y.; Yomogida, Y.; Izadi-Najafabadi, A.; Futaba, D. N.; Hata, K. A Stretchable Carbon Nanotube Strain Sensor for Human-Motion Detection. *Nat. Nanotechnol.* **2011**, *6*, 296−301.

(3) Wang, X.; Liu, Z.; Zhang, T. Flexible Sensing Electronics for Wearable/Attachable Health Monitoring. *Small* **2017**, *13*, 1−19.

(4) Pang, C.; Lee, C.; Suh, K.-Y. Recent Advances in Flexible Sensors for Wearable and Implantable Devices. *J. Appl. Polym. Sci.* **2013**, *130*, 1429−1441.

(5) Luo, N.; Dai, W.; Li, C.; Zhou, Z.; Lu, L.; Poon, C. C. Y.; Chen, S. C.; Zhang, Y.; Zhao, N. Flexible Piezoresistive Sensor Patch Enabling Ultralow Power Cuffless Blood Pressure Measurement. *Adv. Funct. Mater.* **2016**, *26*, 1178−1187.

(6) Matsuzaki, R.; Todoroki, A. Wireless Flexible Capacitive Sensor Based on Ultra-Flexible Epoxy Resin for Strain Measurement of Automobile Tires. *Sens. Actuators, A* **2007**, *140*, 32−42.

(7) Gullapalli, H.; Vemuru, V. S. M.; Kumar, A.; Botello-Mendez, A.; Vajtai, R.; Terrones, M.; Nagarajaiah, S.; Ajayan, P. M. Flexible Piezoelectric ZnO-Paper Nanocomposite Strain Sensor. *Small* **2010**, *6*, 1641−1646.

(8) Huang, H. Flexible Wireless Antenna Sensor: A Review. *IEEE Sens. J.* **2013**, *13*, 3865−3872.

(9) Xu, X.; Huang, H. Battery-Less Wireless Interrogation of Microstrip Patch Antenna for Strain Sensing. *Smart Mater. Struct.* **2012**, *21*, No. 125007.
(10) Song, L.; Myers, A. C.; Adams, J. J.; Zhu, Y. Stretchable and Reversibly Deformable Radio Frequency Antennas Based on Silver Nanowires. *ACS Appl. Mater. Interfaces* **2014**, *6*, 4248−4253.
(11) Jun, J.; Oh, J.; Shin, D. H.; Kim, S. G.; Lee, J. S.; Kim, W.; Jang, J. Wireless, Room Temperature Volatile Organic Compound Sensor Based on Polypyrrole Nanoparticle Immobilized Ultrahigh Frequency Radio Frequency Identification Tag. *ACS Appl. Mater. Interfaces* **2016**, *8*, 33139−33147.
(12) Nag, A.; Mukhopadhyay, S. C.; Kosel, J. Wearable Flexible Sensors: A Review. *IEEE Sens. J.* **2017**, *17*, 3949−3960.
(13) Reig, C.; Avila-Navarro, E. Printed Antennas for Sensor Applications: A Review. *IEEE Sens. J.* **2014**, *14*, 2406−2418.
(14) Mohammad, I.; Huang, H. An Antenna Sensor for Crack Detection and Monitoring. *Adv. Struct. Eng.* **2011**, *14*, 47−53.
(15) Rai, T.; Dantes, P.; Bahreyni, B.; Kim, W. S. A Stretchable RF Antenna with Silver Nanowires. *IEEE Electron Device Lett.* **2013**, *34*, 544−546.
(16) Pan, L.; Chortos, A.; Yu, G.; Wang, Y.; Isaacson, S.; Allen, R.; Shi, Y.; Dauskardt, R.; Bao, Z. An Ultra-Sensitive Resistive Pressure Sensor Based on Hollow-Sphere Microstructure Induced Elasticity in Conducting Polymer Film. *Nat. Commun.* **2014**, *5*, No. 3002.
(17) Gan, Q.; Qin, N.; Zhu, Y.; Huang, Z.; Zhang, F.; Gu, S.; Xie, J.; Zhang, K.; Lu, L.; Lu, Z. Polyvinylpyrrolidone-Induced Uniform Surface-Conductive Polymer Coating Endows Ni-Rich Li-$Ni_{0.8}Co_{0.1}Mn_{0.1}O_2$ with Enhanced Cyclability for Lithium-Ion Batteries. *ACS Appl. Mater. Interfaces* **2019**, *11*, 12594−12604.
(18) Staaf, L. G. H.; Lundgren, P.; Enoksson, P. Present and Future Supercapacitor Carbon Electrode Materials for Improved Energy Storage Used in Intelligent Wireless Sensor Systems. *Nano Energy* **2014**, *9*, 128−141.
(19) Gao, L.; Wang, Y.; Hu, X.; Zhou, W.; Cao, K.; Wang, Y.; Wang, W.; Lu, Y. Cellular Carbon-Film-Based Flexible Sensor and Waterproof Supercapacitors. *ACS Appl. Mater. Interfaces* **2019**, *11*, 26288−26297.
(20) Jian, M.; Wang, C.; Wang, Q.; Wang, H.; Xia, K.; Yin, Z.; Zhang, M.; Liang, X.; Zhang, Y. Advanced Carbon Materials for Flexible and Wearable Sensors. *Sci. China Mater.* **2017**, *60*, 1026−1062.
(21) Salim, N. V.; Mateti, S.; Cizek, P.; Hameed, N.; Parameswaranpillai, J.; Fox, B. Large, Mesoporous Carbon Nanoparticles with Tunable Architectures for Energy Storage. *ACS Appl. Nano Mater.* **2019**, *2*, 1727−1736.
(22) Li, J.-C.; Xiao, F.; Zhong, H.; Li, T.; Xu, M.; Ma, L.; Cheng, M.; Liu, D.; Feng, S.; Shi, Q.; et al. Secondary-Atom-Assisted Synthesis of Single Iron Atoms Anchored on N-Doped Carbon Nanowires for Oxygen Reduction Reaction. *ACS Catal.* **2019**, *9*, 5929−5934.
(23) Wajahat, M.; Lee, S.; Kim, J. H.; Chang, W. S.; Pyo, J.; Cho, S. H.; Seol, S. K. Flexible Strain Sensors Fabricated by Meniscus-Guided Printing of Carbon Nanotube-Polymer Composites. *ACS Appl. Mater. Interfaces* **2018**, *10*, 19999−20005.
(24) Wu, S.; Lin, Y.; Xing, L.; Sun, G.; Zhou, H.; Xu, K.; Fan, W.; Yu, L.; Li, W. Stabilizing $LiCoO_2$/Graphite at High Voltages with an Electrolyte Additive. *ACS Appl. Mater. Interfaces* **2019**, *11*, 17940−17951.
(25) Castro Neto, A. H.; Guinea, F.; Peres, N. M. R.; Novoselov, K. S.; Geim, A. K. The Electronic Properties of Graphene. *Rev. Mod. Phys.* **2009**, *81*, 109−162.
(26) Geim, A. K. Graphene: Status and Prospects. *Science* **2009**, *324*, 1530−1535.
(27) Xu, Y.; Bai, H.; Lu, G.; Li, C.; Shi, G. Flexible Graphene Films via the Filtration of Water-Soluble Noncovalent Functionalized Graphene Sheets. *J. Am. Chem. Soc.* **2008**, *130*, 5856−5857.
(28) Zhu, Y.; Murali, S.; Cai, W.; Li, X.; Suk, J. W.; Potts, J. R.; Ruoff, R. S. Graphene and Graphene Oxide: Synthesis, Properties, and Applications. *Adv. Mater.* **2010**, *22*, 3906−3924.
(29) Yao, B.; Chen, J.; Huang, L.; Zhou, Q.; Shi, G. Base-Induced Liquid Crystals of Graphene Oxide for Preparing Elastic Graphene Foams with Long-Range Ordered Microstructures. *Adv. Mater.* **2016**, *28*, 1623−1629.
(30) Wang, Y.; Yao, B.; Chen, H.; Wang, H.; Li, C.; Yang, Z. Preparation of Anisotropic Conductive Graphene Aerogel/Polydimethylsiloxane Composites as LEGO Modulars. *Eur. Polym. J.* **2019**, *112*, 487−492.
(31) Wu, H.; Drzal, L. T. Graphene Nanoplatelet Paper as a Light-Weight Composite with Excellent Electrical and Thermal Conductivity and Good Gas Barrier Properties. *Carbon* **2012**, *50*, 1135−1145.
(32) Xin, G.; Sun, H.; Hu, T.; Fard, H. R.; Sun, X.; Koratkar, N.; Borca-Tasciuc, T.; Lian, J. Large-Area Freestanding Graphene Paper for Superior Thermal Management. *Adv. Mater.* **2014**, *26*, 4521−4526.
(33) Teng, C.; Xie, D.; Wang, J.; Yang, Z.; Ren, G.; Zhu, Y. Ultrahigh Conductive Graphene Paper Based on Ball-Milling Exfoliated Graphene. *Adv. Funct. Mater.* **2017**, *27*, No. 1700240.
(34) Xia, W.; Zhang, B.; Zhou, W.; Zhang, J.; Liu, C.; He, D.; Wu, Z. P. In *Rectangular Dielectric Resonator Antenna Fed by Offset Tapered Copper and Graphene Microstrip Lines for 5G Communication*, 2018 IEEE International Conference on Computational Electromagnetics (ICCEM), 2018.
(35) Wang, Z.; Mao, B.; Wang, Q.; Yu, J.; Dai, J.; Song, R.; Pu, Z.; He, D.; Wu, Z.; Mu, S. Ultrahigh Conductive Copper/Large Flake Size Graphene Heterostructure Thin-Film with Remarkable Electromagnetic Interference Shielding Effectiveness. *Small* **2018**, *14*, No. 1704332.
(36) Zhang, N.; Wang, Z.; Song, R.; Wang, Q.; Chen, H.; Zhang, B.; Lv, H.; Wu, Z.; He, D. Flexible and Transparent Graphene/Silver-Nanowires Composite Film for High Electromagnetic Interference Shielding Effectiveness. *Sci. Bull.* **2019**, *64*, 540−546.
(37) Zhou, W.; Liu, C.; Song, R.; Zeng, X.; Li, B. W.; Xia, W.; Zhang, J.; Huang, G. L.; Wu, Z. P.; He, D. Flexible Radiofrequency Filters Based on Highly Conductive Graphene Assembly Films. *Appl. Phys. Lett.* **2019**, *114*, No. 113503.
(38) Tang, D.; Wang, Q.; Wang, Z.; Liu, Q.; Zhang, B.; He, D.; Wu, Z.; Mu, S. Highly Sensitive Wearable Sensor Based on a Flexible Multi-Layer Graphene Film Antenna. *Sci. Bull.* **2018**, *63*, 574−579.
(39) Chen, H. D. Broadband CPW-Fed Square Slot Antennas with a Widened Tuning Stub. *IEEE Trans. Antennas Propag.* **2003**, *51*, 1982−1986.
(40) Kanaparthi, S.; Sekhar, V. R.; Badhulika, S. Flexible, Eco-Friendly and Highly Sensitive Paper Antenna Based Electromechanical Sensor for Wireless Human Motion Detection and Structural Health Monitoring. *Extrem. Mech. Lett.* **2016**, *9*, 324−330.
(41) Ramadan, M.; Dahle, R. Characterization of 3-D Printed Flexible Heterogeneous Substrate Designs for Wearable Antennas. *IEEE Trans. Antennas Propag.* **2019**, *67*, 2896−2903.
(42) Moradi, B.; Martinez, M.; Fernández-García, R.; Gil, I. Wearable Ring Resonator Antenna. *Phys. Status Solidi Appl. Mater. Sci.* **2018**, *215*, No. 1800410.
(43) Song, R.; Huang, G.-L.; Liu, C.; Zhang, N.; Zhang, J.; Liu, C.; Wu, Z. P.; He, D. High-Conductive Graphene Film Based Antenna Array for 5G Mobile Communications. *Int. J. RF Microw. Comput. Eng.* **2019**, *29*, No. e21692.
(44) Zhou, W.; Liu, C.; Huang, G.-L.; Xia, W.; Zhang, J.; He, D.; Wu, Z. Design and Manufacture of Lowpass Microstrip Filter with High Conductivity Graphene Films. *Microw. Opt. Technol. Lett.* **2019**, *61*, 972−978.


https://dx.doi.org/10.1021/acsomega.0c00263
*ACS Omega* 2020, 5, 12937−12943